Physical Chemistry Chemical Physics

PCCP

Geometry of the magic number H+(H2O)21 water cluster by proxy

Journal:	*Physical Chemistry Chemical Physics*
Manuscript ID:	CP-ART-11-2014-005246.R2
Article Type:	Paper
Date Submitted by the Author:	07-Jan-2015
Complete List of Authors:	Ryding, Mauritz; University of Oslo, Department of Chemistry Izsák, Róbert; Max-Planck Institute for Chemical Energy Conversion, Merlot, Patrick; University of Oslo, Reine, Simen; University of Oslo, Helgaker, Trygve; University of Oslo, Uggerud, Einar; University of Oslo, Department of Chemistry

Geometry of the magic number $H^+(H_2O)_{21}$ water cluster by proxy

Mauritz Johan Ryding,[1,*] Róbert Izsák,[2] Patrick Merlot,[3] Simen Reine,[3] Trygve Helgaker[3] and Einar Uggerud[1,*]

[1] Mass Spectrometry Laboratory and Centre for Theoretical and Computational Chemistry (CTCC), Department of Chemistry, University of Oslo, P. O. B. 1033 Blindern, NO-0315 Oslo, Norway.

[2] Max-Planck-Institut für Chemische Energiekonversion, Stiftstr. 34-36, DE-45470 Mülheim an der Ruhr, Germany.

[3] Centre for Theoretical and Computational Chemistry (CTCC), Department of Chemistry, University of Oslo, P. O. B. 1033 Blindern, NO-0315 Oslo, Norway.

* Corresponding authors:

Mauritz.ryding@kjemi.uio.no

einar.uggerud@kjemi.uio.no

Abstract

Abundance mass spectra obtained upon carefully electrospraying solutions of *tert*-butanol (TB) in water into a mass spectrometer displays a systematic series of peaks due to mixed $H^+(TB)_m(H_2O)_n$ clusters. Clusters with $m + n = 21$ have higher abundance (magic number peaks) than their neighbours when $m \leq 9$, while for $m > 9$ they have lower abundance. This indicates that the mixed TB/H_2O clusters retain a core hydrogen bonded network analogous to that in the famous all-water $H^+(H_2O)_{21}$ cluster up to the limit $m = 9$. The limiting value corresponds to the number of dangling O–H groups pointing out from the surface of the degenerated pentagonal dodecahedral, considered to be the lowest energy form of $H^+(H_2O)_{21}$; the experimental findings therefore supports this geometry. The experimental findings are supported by ab initio quantum chemical calculations to provide a consistent framework for the interpretation of experiments of this kind.

Introduction

Gas hydrates are naturally occurring inclusion compounds in which the guest molecule (CH_4, CO_2, *etc.*) is trapped in a cage formed by a lattice of host molecules of water. Such compounds are termed clathrates and were described by Davy already in 1810 (for a review, see Michael Faradays "Experimental Researches in Chemistry and Physics").[1] In 1949, von Stackelberg noticed that clathrates tend to crystallise in the cubic crystal system, in contrast to pure water which forms hexagonal ice.[2] To account for the contents of the unit cells of clathrates, a structural arrangement in which the water molecules form cyclic hydrogen bonded networks in the form of pentagons was suggested by Claussen in 1951.[3] Among the geometrical arrangements formed in this manner, the most noticeable is the pentagonal dodecahedron (often denoted 5^{12}), one of the five Platonic solids, where each oxygen atom of the constituent twenty water molecules occupies one apex. The void of the resulting cage is sufficiently large to hold one or several guest molecules, thereby giving rise to a stable solid structure. In a similar manner, it has been shown that the 5^{12} structure may be present inside the nano-cavities of certain solid molybdenum oxides.[4] A topological analysis of the most favourable hydrogen bond pattern that can be achieved in isolated clusters of the type $(H_2O)_{20}$, while maximizing the number of O–H···O bonds, reveals that 10 O–H bonds point outwards without engaging in hydrogen bonding. In addition to these dangling O–H bonds, the 5^{12} structure is characterised by the pentagonal angle of 108.0 degrees, less than the tetrahedral angle of 109.4 degrees. The pentagon therefore offers a slightly better fit to a water molecule than does the hexagon, as a free water molecule has an inherent H–O–H angle of 104.5 degrees (as a compromise, the H–O–H angle in hexagonal ice is 106.6 degrees).[5]

The development of new experimental techniques in the early 1970s made it possible to investigate ionic water clusters using mass spectrometry. In 1973, Lin demonstrated

that a wide distribution of $H^+(H_2O)_n$ ions is formed by supersonic expansion of water vapour into vacuum.[6] Remarkably, the n = 21 cluster is clearly more abundant than its neighbours in the mass spectrum.[6-9] Such magic numbers are also seen for n = 28 and 55. In the present study, we attempt to further elucidate the delicate issue of the structural nature of these magic numbers.

Magic numbers had been foreseen by Hagen and Kassner in 1969, who suggested a clathrate structure for $H^+(H_2O)_{21}$, in which the hydronium ion, H_3O^+, occupies the void of the $(H_2O)_{20}$ pentagonal dodecahedral cage.[10, 11] More recently, quantum chemical calculations have modified this picture. Fully optimized geometries show a distorted dodecahedral molecular arrangement, in which the hydronium ion is part of the cage, while a H_2O molecule sits on the inside.[12-16]

In the case of protonated water, it is a general observation that the magic numbers at n = 21, 28 and 55 can be obtained irrespective of the method by which one produces the cluster distribution; for example, by supersonic expansion or electrospray ionization.[7, 17] While a common interpretation is that the magic number clusters are inherently more stable than their neighbours, there is also evidence that they appear due to a higher instability of the next larger cluster and thus arise from variations in evaporation rate with cluster size.[17, 18] The low cluster temperatures mean that the entropy term is of minor significance—in other words, it seems that clusters formed at such low temperatures are solid-like rather than liquid-like, and that the concept of structure is a meaningful one under these conditions. However, one also has to keep in mind that the cluster distributions are affected by kinetic factors, since fast cooling may lead to the cluster being trapped in a thermodynamically less stable form. It should finally be noted that proton scrambling experiments show that the clusters exhibit a high degree of intra-cluster proton mobility despite the low temperature.[19, 20]

Currently, there exist few direct methods for structure determination of small ionic clusters in the isolated gaseous state, electron diffraction being an exception. The experimentalist is therefore often depending upon indirect evidence. From infrared action spectroscopy, it is possible to identify spectral features corresponding to dangling O–H bonds,[21, 22] and also spectral features indicative of the hydronium ion embedded on the surface of the cage.[23] A completely different approach to the structural features was taken by Castleman and co-workers,[24] who elegantly performed titration experiments between $H^+(H_2O)_{21}$ and trimethylamine (TMA). It was demonstrated that, for the clusters $H^+(TMA)_m(H_2O)_{21}$, up to 10 TMA molecules may be added, and the cluster would still be magic. Castleman and co-workers thereby concluded that $H^+(H_2O)_{21}$ would have 10 dangling O–H groups, with H_3O^+ in the centre of the cluster. The only caveat is that the current "consensus" structure of $H^+(H_2O)_{21}$ has 9 rather than 10 dangling O–H bonds, and that the core H_3O^+ ion is found at the surface. In a second study from the same laboratory, mixed $H^+(CH_3OH)_x(H_2O)_y$ clusters were produced with up to 13 methanol molecules; a systematic enhancement of abundance was observed for $x + y = 21$ when $x \leq 8$.[25] However, the enhancements become less distinct as x increases and at $x = 8$ it is just discernible. Nevertheless, this observation indicates some conservation of the cluster structure and hydrogen bond pattern as water molecules are being replaced by CH_3OH and hence that each methyl group substitutes one dangling hydrogen. However, it was not possible to determine whether 8 substitutions with methanol molecules actually corresponds to the number of dangling O–H units in the magic $H^+(H_2O)_{21}$ cluster. If so, the structure would be different from both the trimethylamine titration experiment and the consensus geometry. The compatibility of water and methanol in mixed clusters, and their ability to form magic-number clusters by successive replacement of water by methanol, is also corroborated by IR spectroscopy experiments.[26]

To probe deeper into this fascinating structural enigma, we decided to perform an alcohol/water mixed cluster experiment similar to that of Castleman but using tertiary butanol (TB) instead of methanol. The idea is that the hydroxyl "head" of TB will replace the O–H part of a surface water molecule, and that the tert-butyl group will replace the dangling hydrogen. Thus, we hypothesize that the larger size and the hydrophobicity of the alkyl group will lead to clearer trends in the magic number patterns due to the likely preference of this group for the exterior rather than the interior of the clusters, while keeping the core structure intact. An important difference relative to the experiments involving TMA[24] is that the dangling hydrogen atoms will be replaced rather than bonded to. The present study also involves quantum chemical calculations of protonated mixed TB/water clusters to investigate if substitution of dangling hydrogens with tert-butyl groups leads to stable cluster structures with the core intact, as suggested in the paragraph above. For the same purpose, we have also conducted calculations of adducts between $H^+(H_2O)_{21}$ and TMA. The hope is that these calculations will help us interpret the results of previous and current experiments in terms of one unifying structural concept.

Results

Experimental results

The experiments were conducted using a quadrupole–time-of-flight (QTOF) mass spectrometer; see the Section Experimental methods for details.

A mass spectrum (Fig. 1) covering the range 0–1000 Th, obtained from a water solution containing 30 mM TB, shows cluster size distributions identified as $H^+(H_2O)_n$, $H^+(TB)_1(H_2O)_n$, $H^+(TB)_2(H_2O)_n$ and $H^+(TB)_3(H_2O)_n$. The overall distributions of the three latter series are in most aspects similar to the distribution of $H^+(H_2O)_n$, which has been

reported previously for this instrument.[20] In addition to the above mentioned series of clusters, the protonated TB dimer and trimer give rise to large peaks in the spectrum; the protonated tetramer has a very small peak, while the protonated monomer is hardly observed at all. The tert-butyl cation $C_4H_9^+$ is observed to some small extent.

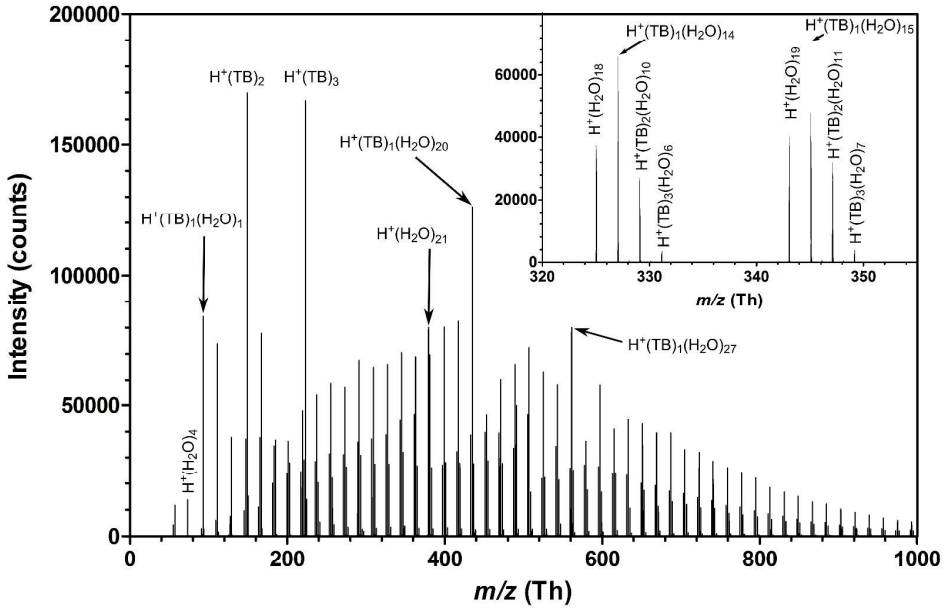

Figure 1. Mass spectrum showing a cluster distribution formed from electrospraying a solution of 30 mM tert-butyl alcohol (TB) in water. The inset shows a magnification of the region m/z = 320–355 Th.

To better visualise intensity variations with size for different cluster series, the peaks in the distribution spectra (Fig. 1) were integrated. Each series— $H^+(H_2O)_n$, $H^+(TB)_1(H_2O)_n$, $H^+(TB)_2(H_2O)_n$ and $H^+(TB)_3(H_2O)_n$—is presented as a separate curve in the abundance spectrum in Fig. 2; they are given on a logarithmic scale as a function of the number of water molecules, n, in the cluster.

The pure water clusters $H^+(H_2O)_n$ shown in Fig. 2 exhibit the well-known magic numbers at n = 21 and 28. These are followed, respectively, by the "anti-magic" clusters n = 22 and 29. The agreement with previous measurements of $H^+(H_2O)_n$ is excellent.[20] The most striking features of Fig. 2 are the magic numbers of the mixed TB–H_2O clusters. These reproduce the magic numbers of the pure water clusters, except that they appear at one value of n lower for each TB present in the cluster. We conclude that the magic numbers $H^+(TB)_m(H_2O)_n$ appear at $m + n$ = 21, 28 *etc.*, analogous to the results for $H^+(CH_3OH)_m(H_2O)_n$ reported by Castleman and co-workers.[25]

A second point of interest in Fig. 2 is the emergence of an additional weak magic number. The region n = 22–27 is, for the pure water cluster (m = 0), rather smooth. As the number of TB in the clusters increases, this region between the two major magic numbers becomes more jagged. A minor magic number appears for $H^+(TB)_3(H_2O)_{22}$, corresponding to $m + n$ = 25.

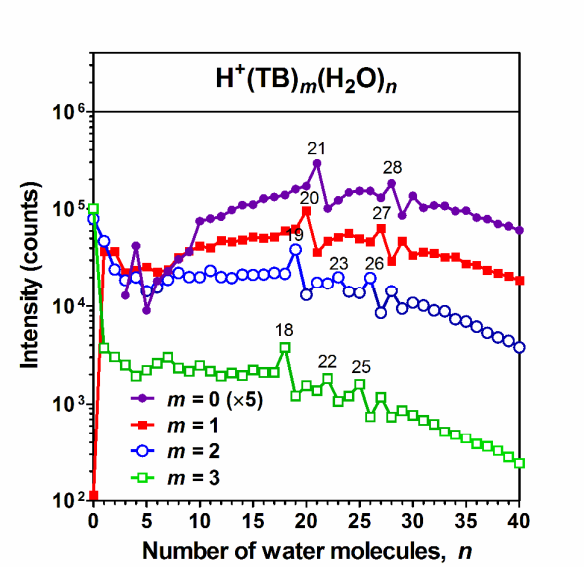

Figure 2. Abundance of $H^+(TB)_m(H_2O)_n$ clusters with m = 0–3 in a QTOF spectrum produced from a solution of 30 mM tert-butyl alcohol (TB) in water; data presented as a function of the number

of water clusters in the cluster, *n* (some values of which is indicated in the figure). The curve for $H^+(H_2O)_n$ is multiplied by 5 for ease of comparison.

As indicated in the Introduction, a shortcoming of the methanol/water cluster study of Castleman[25] is that it is hard to determine where the saturation limit is with regards to replacing all dangling hydrogens of $H^+(H_2O)_{21}$ with methyl groups. In the hope that clearer trends could be obtained using TB instead of methanol, we worked out experimental conditions to increase the relative number of TB molecules in the clusters so as to probe the upper limit of H_2O replacement by TB for the magic numbers.

Using a more concentrated solution of 250 mM TB in water allowed us to also measure the abundance distribution of clusters containing up to and including 11 TB molecules; unfortunately, this also resulted in poor intensity for clusters with 0–3 TB molecules. In a few instances, even peaks corresponding to $H^+(TB)_{12}(H_2O)_n$ could be discerned; however, this data set was incomplete and deemed too unreliable for inclusion here. Figure 3 displays the abundance of clusters containing 4–11 TB molecules as a function of the total number of TB and H_2O molecules in the cluster ($m + n$, respectively) from 17 to 35. A separate measurement performed using a 250 mM TB solution, but with a reduced flow of solution to the electrospray, resulted in sufficiently good abundance of clusters in the range $m = 0–10$, but not for $n = 11$; that measurement can be seen in the Supplementary Information.

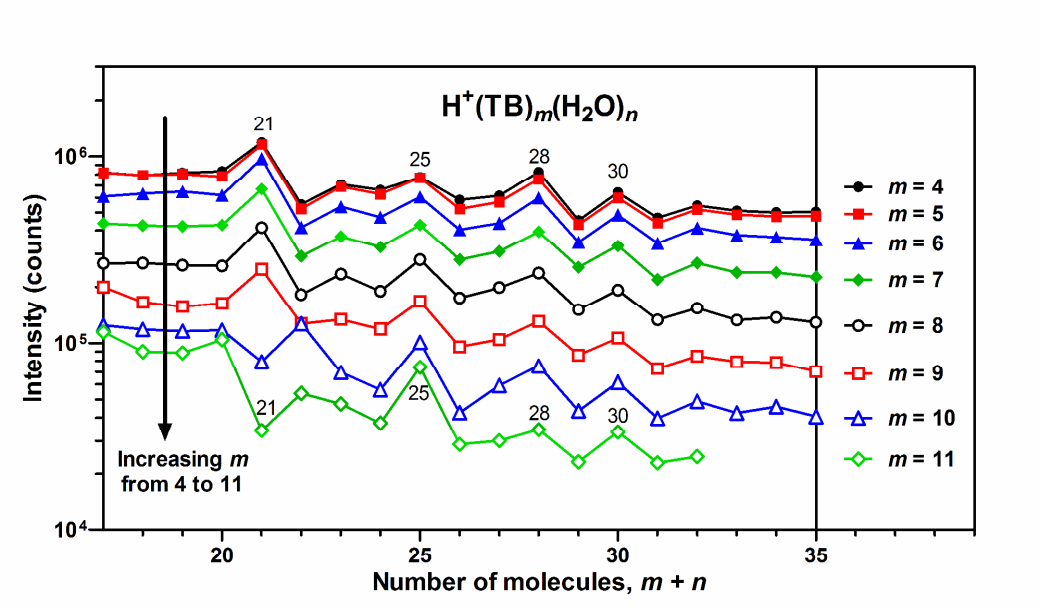

Figure 3. Abundance of $H^+(TB)_m(H_2O)_n$ clusters with m = 4–11 in a QTOF spectrum produced from a solution of 250 mM tert-butyl alcohol (TB) in water; data presented as a function of the total number of molecules in the cluster, $m + n$.

As seen in Fig. 3, magic numbers are observed for $m + n$ = 21, 28 and 30 in all of the cluster series, with the exception that the combination $m + n$ = 21 results in magic clusters only up to m = 9. For m = 10–11, we find that $m + n$ = 21 is not a magic number; on the contrary, $H^+(TB)_{10}(H_2O)_{11}$ and $H^+(TB)_{11}(H_2O)_{10}$ can be described as being anti-magic clusters. We also see the previously mentioned magic number $m + n$ = 25 becoming increasingly more prominent as m increases.

These results are a clear indication that up to nine TB molecules are able to replace H_2O in mixed TB/water clusters without affecting the properties that make the 21 molecule cluster particularly abundant; however, a tenth (or even eleventh) TB molecule cannot be properly accommodated, resulting instead in a less stable cluster. Interestingly, for the m = 10 series, the $m + n$ = 22 cluster appears to be more stable. Once the members of

the m = 10 and m = 11 series increase in size beyond this point (*i.e.* contain more water molecules), there is little or no difference from the other cluster series.

Overall, the experimental results fit excellently to the picture of a size 21 cluster originally having nine dangling hydrogen atoms that can be replaced with tert-butyl groups without altering the internal cluster structure, while a tenth TB molecule cannot be incorporated. As the number of water molecules in the original cluster increases beyond 21–22, additional dangling hydrogens become available for replacement by tert-butyl. At this point, a tenth TB molecule can replace H_2O without altering the internal cluster structure, as evident by the fact that $H^+(TB)_{10}(H_2O)_n$ and $H^+(TB)_{11}(H_2O)_n$ exhibits the same $m + n$ = 25, 28 and 30 magic numbers as clusters containing 0–9 TB molecules.

A collision-induced dissociation measurement was performed on the $H^+(TB)_{10}(H_2O)_{11}$ cluster and on the $H^+(TB)_{10}(H_2O)_{12}$ cluster to see if the collision products would include loss of TB from the cluster. However, the results—which can be viewed in the Supplementary Information—clearly show that the preferred collision-induced dissociation product was loss of one or two H_2O molecules, with the loss of TB being a very minor product.

Computational results

The computational results are presented in Fig. S4 (in the Supplementary Information) and in Figs. 4–6. The Supplementary Information also contains larger versions of Figs. 4–6 and Cartesian coordinates for the presented structures. In addition, Gaussian output files (.out) containing the structures are available; these files can be viewed using *Jmol* (an open-source Java viewer for chemical structures in 3D).[27]

A geometry optimization was conducted for the $H^+(H_2O)_{21}$ cluster, based upon the lowest energy form from the work by Kus *et al.*[15]. The resulting cluster geometry and electrostatic potential mapping are shown in Fig. S4 in the Supplementary Information, where also a more thorough discussion on the geometry is given. As already emphasized, the optimum molecular arrangement of the $H^+(H_2O)_{21}$ cluster comprises a total of 9 dangling O–H groups, in contrast to the situation in the clathrate $(H_2O)_{20}$, which has 10. The H_3O^+ entity embedded in the degenerated pentagonal dodecahedron surface within $H^+(H_2O)_{21}$ defines a natural centre of the molecular assembly. A study of the electrostatic potential mapping of the cluster (Fig. S4) reveals that the hydronium ion occupies the centre of the most electronegative region together with the three water molecules directly interacting with it. The rest of the surface is more positive, with distinct positive potential values around the dangling hydrogen atoms. Thus, the region of the cluster around the hydronium ion is distinctively nucleophilic and the positive charge is smeared out over the rest of the cluster surface; this is in contrast to how we write the condensed formula, $H^+(H_2O)_{21}$ or $H_3O^+(H_2O)_{20}$, which implies a positive charge-carrying core ion in an otherwise electrically neutral medium.

We now turn our attention to the mixed TB/water cluster $H^+(TB)_9(H_2O)_{12}$. As mentioned in the experimental section, this is the $m + n = 21$ cluster containing the maximum number of TB molecules while remaining a magic number. The geometry of the molecular arrangement was obtained by starting the optimization from a geometry where the hydrogen atoms of all 9 dangling O–H groups of $H^+(H_2O)_{21}$ were substituted by tert-butyl groups. The resulting geometry is reproduced in Fig. 4.

Given that the $H^+(H_2O)_{21}$ cluster is most likely to have nine dangling hydrogen bonds and that $H^+(TB)_9(H_2O)_{12}$ is a magic number cluster, we expect the latter to have a surface that is saturated with regards to the replacement of dangling hydrogens by tert-butyl

groups while retaining the hydrogen bond network of the former—that is, we expect the final optimized structure to be essentially the same as the initial structure. This is clearly the case, as seen in Fig. 4. Nevertheless, it should be mentioned that while the optimized $H^+(TB)_9(H_2O)_{12}$ structure presented here is most likely the global minimum, an exhaustive search was not attempted.

Importantly, the H_3O^+ moiety in $H^+(TB)_9(H_2O)_{12}$ retains its integrity in the calculated structure—even though the TB molecule in its free form has a substantially higher proton affinity than the water molecule—implying that synergism in the H-bond network is essential to the stability of these structures. The distribution of electrostatic potential here shows a similar pattern to that of the water cluster $H^+(H_2O)_{21}$ (Fig. S4): the hydronium ion and its immediate partners occupy the most negative region. Upon inspection of the calculated geometry of the $H^+(TB)_9(H2O)_{12}$ cluster, it is evident that the void in the surface tert-butyl layer above H_3O^+, which would be the space available to a tenth tert-butyl group, is just slightly larger than the average surface area available to the nine tert-butyl groups already present.

From these results, it becomes evident that the replacement of a tenth water molecule by TB, giving the $H^+(TB)_{10}(H_2O)_{11}$ cluster, will require a drastic alteration of the core structure by breaking hydrogen bonds. The resulting hydrogen bond network will thus no longer resemble that of $H^+(H_2O)_{21}$, in agreement with the experimental results of $H^+(TB)_{10}(H_2O)_{11}$ not being a magic number.

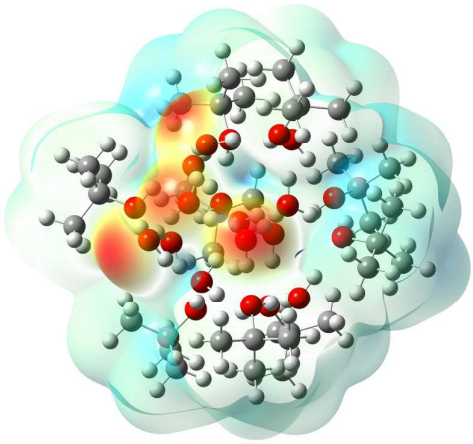

Figure 4. Isodensity plot mapping the electrostatic potential, indicating electronegative (red) and electropositive (blue) areas of the geometry optimized $H^+(TB)_9(H_2O)_{12}$ cluster. Colours indicating intermediate charge values have been faded to enhance visibility.

Finally, we discuss the "titration" experiments with TMA mentioned in the Introduction. Figure 5 shows the optimized structure of $H^+(TMA)_9(H_2O)_{21}$: the result of letting 9 TMA molecules accept a hydrogen bond from each of the dangling O–H groups of the most stable $H^+(H_2O)_{21}$ cluster. Again, this structure retains its H_3O^+ core, which exhibits a nucleophilic rather than electrophilic character. The variation in the potential, as indicated by the darker overall shade of the surface, is smaller than for $H^+(H_2O)_{21}$ (Fig. S4) or $H^+(TB)_9(H_2O)_{12}$ (Fig. 4).

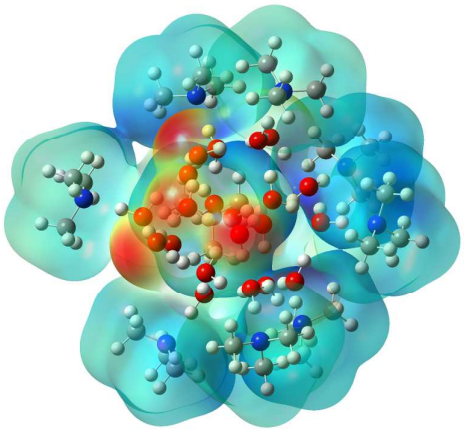

Figure 5. Isodensity plot mapping the electrostatic potential, indicating electronegative (red) and electropositive (blue) areas of the geometry optimized $H^+(TMA)_9(H_2O)_{21}$ cluster. Colours indicating intermediate charge values have been faded to enhance visibility.

Most of the surface of $H^+(TMA)_9(H_2O)_{21}$ is covered by the nine TMA molecules; thus, an incoming tenth TMA molecule is unlikely to be bound there. The remaining possibility is for TMA to attack the nucleophilic centre, assuming that it has sufficient energy to overcome the initial repulsion. Forcing a tenth TMA molecule in a position immediately above one of the hydrogens of the H_3O^+ moiety (r_{N-H} = 1.5 Å) and reoptimizing the geometry reveals an interesting phenomenon; the incoming tenth TMA is able to disrupt the hydrogen bond network, extract, and finally abstract one of the three hydrogens. The resulting $(CH_3)_3HN^+$ moiety remains hydrogen-bonded to the water molecule left over from the hydronium ion, while the hydrogens on one of the TMA methyl groups form hydrogen bonds to an adjacent water molecule, leading to the $H^+(TMA)_{10}(H_2O)_{21}$ (geometry A) structure depicted in Fig. 6.

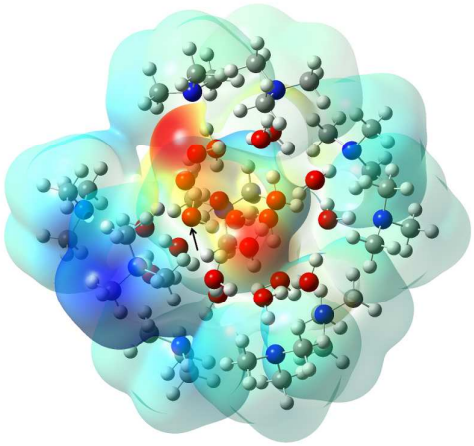

Figure 6. Isodensity plot mapping the electrostatic potential, indicating electronegative (red) and electropositive (blue) areas of the geometry optimized $H^+(TMA)_{10}(H_2O)_{21}$ (geometry A) cluster. The arrow indicates what used to be the hydronium ion in the structure. Colours indicating intermediate charge values have been faded to enhance visibility.

If we for $H^+(TMA)_{10}(H_2O)_{21}$ instead start from a larger N–hydronium distance (r_{N-H} = 2 Å), then the TMA molecule is pushed further out, leaving the $H^+(H_2O)_{21}$ core intact. This results in a structure $H^+(TMA)_{10}(H_2O)_{21}$ (geometry B), which is essentially the same as $H^+(TMA)_9(H_2O)_{21}$ with the very weakly bound additional TMA molecule at a distance r_{N-H} = 2.8 Å. The 0 K dissociation enthalpies for

$$H^+(TMA)_{10}(H_2O)_{21}\text{ (geometry A)} \rightarrow H^+(TMA)_9(H_2O)_{21} + TMA \quad (1)$$

and

$$H^+(TMA)_{10}(H_2O)_{21}\text{ (geometry B)} \rightarrow H^+(TMA)_9(H_2O)_{21} + TMA \quad (2)$$

are 54 and 8 kJ mol^{-1}, respectively. The former value is close to the 57 kJ mol^{-1} computed separately for

$$H^+(TMA)_9(H_2O)_{21} \rightarrow H^+(TMA)_8(H_2O)_{21} + TMA, \quad (3),$$

which is the energy needed to remove one TMA molecule from the stable $H^+(H_2O)_{21}(TMA)_9$ complex. This observation indicates the existence of a stable structure that can accommodate a tenth TMA molecule. Since the formation of the TMA-containing clusters are not by equilibration, it is unclear how difficult it is to overcome the repulsive barrier of the nucleophilic site. However, it should be remembered that under experimental conditions, formation of, *e.g.*, $H^+(H_2O)_{21}(TMA)_{10}$ (geometry A) does not necessarily occur through addition of TMA to $H^+(H_2O)_{21}(TMA)_9$, which may circumvent the need to overcome the barrier. Clusters can for instance be formed by evaporation of

molecules from larger clusters, again with the risk that fast cooling may lead to the freezing out of more stable geometries.

Experimental methods

The experiments were performed using a quadrupole–time-of-flight mass spectrometer (QTOF2, Micromass/Waters, Manchester UK), used previously for the study of several aqueous clusters.[18, 20, 28-31] Solutions of TB in water (30 mM and 250 mM) were fed to the Z-configuration electrospray ionisation source operating at room temperature and with reduced gas flows. Flow rates of solution to the electrospray ion source were 20–30 μL min^{-1}. The produced $H^+(TB)_m(H_2O)_n$ ions were transferred from the atmospheric pressure environment of the electrospray source via a differentially pumped stage (a few mbar) to the high vacuum part of the instrument. At this point, the clusters cease to be heated by collisions with gas molecules, becoming instead a meta-stable evaporative ensemble.[32] The clusters then passed through the quadrupole mass filter that was operated in RF-only mode and essentially acting as a ramped high pass filter to minimize bias to different parts of the cluster distribution. After the quadrupole, the clusters' flight path took them through the collision chamber at a nominal collision-energy of 1.0 eV in the lab-frame (the nominal collision-energy corresponds to the kinetic energy of the ion in the direction of the ion beam). The collision cell was kept empty, meaning that no collisions occurred (rest gas collisions will still occur occasionally throughout the instrument high-vacuum compartments). Finally, the cluster distribution entered the time-of-flight (TOF) analyser, which recorded the abundance spectra. The TOF detector is a micro-channel plate detector of the chevron type. The measurements were repeated on separate occasions to verify reproducibility.

Isobaric overlap occurs for some of the peaks of interest in the recorded abundance spectra. Specifically, this becomes a problem for the series $H^+(TB)_9(H_2O)_n$ and

$H^+(H_2O)_{n+37}$ (the mass difference is approximately 0.25 u), and also for $H^+(TB)_{10}(H_2O)_n$ and $H^+(TB)_1(H_2O)_{n+37}$, and so on for larger values of *m*. Fortunately, the mass resolution of the QTOF ($m/\Delta m$ = 5600–6000FWHM for the current measurements) combined with the integration algorithms of the accompanying software (*Masslynx* 4.0) was sufficient to separate the isobaric overlaps into distinct peaks. In the one case where this was not possible (the cluster $m = 2$, $n = 51$ overlapping the cluster $m = 11$, $n = 15$) the peaks were separated by the fitting of gaussian curves to the combined peak shape. The signal-to-noise ratio varies greatly for different peaks, as peak intensity can span several orders of magnitudes. At the worst point, which occurs in the $m = 11$ series presented in Fig. 3, the peak height is approximately 5 times the height of the baseline; although most peaks in this series have a better signal-to-noise ratio. Errors in peak intensity due to statistical fluctuations are generally sufficiently small to be neglected, as the standard deviation equals the square root of the peak intensity (Poisson distribution).

Chemicals: water (HiPerSolv CHROMANORM for HPLC, VWR BDH Prolabo), tert-butyl alcohol (> 99% (GC), Fluka).

Computational methods

All density-functional calculations have been carried out using a development version of the LSDALTON quantum chemistry program,[33] employing the B3LYP exchange–correlation functional[34] together with the D3BJ variant of Grimme's dispersion correction[35] and Pople's 6-31+G* split-valance basis set.[36, 37] The geometry optimizations were carried out in redundant internal coordinates,[38] with a quasi-Newton approach for the geometry steps and with a BFGS update of the Hessian.[39]

For the Hartree term, the density-fitting approach was used with the def2-QZVPP fitting basis of the Karlsruhe group[40] (for details see Reine *et al.*[41]). For the exchange evaluation, a scaled variant of the auxiliary-density-matrix method (ADMM) was used, recently published under the moniker ADMMS.[42] All ADMM approaches require an auxiliary basis set, smaller than the primary orbital basis; we here used the 6-31G* basis set for this purpose.[36] The accuracy of the ADMMS method was tested by performing the optimizations for the smallest cluster with and without this approximation. The difference in geometrical parameters was found to be negligible and much smaller than the changes that occur by neglecting the dispersion correction: the RMSD deviation for bond angles is 0.004 Å vs. 0.03 Å; for bond angles 0.2° vs. 0.5°; for dihedral angles 0.4° vs. 1.3° for ADMM and for the dispersion correction, respectively. Geometry optimizations were converged to 10^{-4} atomic units, using the four convergence criteria as specified in Reine *et al.*;[41] see also the Supplementary Information.

Final Discussion and Conclusions

We have demonstrated that by carefully varying the electrospray conditions and TB solution strength it is possible to produce $H^+(TB)_m(H_2O)_n$ clusters with m = 0–11 from water mixtures containing the alcohol. For these mixed TB/H_2O clusters, magic numbers are found for $m + n$ = 21, 28, 30, and for the larger values of m, also for $m + n$ = 25. The experimental results clearly show that $H^+(TB)_m(H_2O)_n$ clusters with $m + n$ = 21 have higher abundance when $m \leq 9$, while for $m > 9$ they have lower abundance. It therefore appears that these $m + n$ = 21 clusters retain the characteristic degenerated pentagonal dodecahedral core structure of the well-known magic number $H^+(H_2O)_{21}$ cluster, which has nine dangling hydrogen atoms which all may be substituted by tert-butyl groups. Increasing m above this limit would result in a distortion of the core hydrogen bonded network in order to produce what correspond to more dangling bonds in a pure water

cluster; this effect is observed in the experimental results as the anti-magic nature of the clusters where $m + n = 21$ and $m > 9$.

These conclusions are supported by quantum chemical calculations, which show that the tert-butyl groups of $H^+(TB)_9(H_2O)_{12}$ form a tight hydrophobic outside layer, except in the small surface region occupied by the core hydronium ion. Interestingly, and in contrast to the formal electron structure that may be drawn, the hydronium ion region is nucleophilic, demonstrating efficient charge delocalization in the hydrogen bond network.

A previously conducted titration experiment with TMA had indicated that up to 10 TMA molecules can be added to $H^+(H_2O)_{21}$ and the cluster would still be magic. This would correspond to a situation where all nine dangling hydrogens serve as hydrogen bond donors, each to one TMA, and the addition of the tenth TMA molecule would require rearrangement of the core structure, allowing for the formation of a tenth hydrogen bond donor. Our quantum chemical model calculations failed to recover this mechanism, indicating that the rearrangement may be hindered by a considerable activation barrier, in agreement with the observed electron rich character of the hydronium ion that seems to be the most likely candidate site for such a rearrangement. However, our survey is not sufficiently detailed and accurate to allow for a clear conclusion in this respect.

Acknowledgements

The authors wish to acknowledge Prof. José-Luis M. Abboud for stimulating discussions. This work was supported by the Norwegian Research Council by the Grants No. 205512/F20, Nano-solvation in Hydrogen-Bonded Clusters; and No. 179568/V30, to the Centre of Theoretical and Computational Chemistry through their Centre of Excellence

program; and the Norwegian Supercomputing Program (NOTUR) through a grant of computer time (Grant No. NN4654K).

References

1. M. Faraday, *Experimental Researches in Chemistry and Physics*, Taylor and Francis, London, 1859.
2. M. von Stackelberg and H. R. Müller, *Z Elektrochem, Ber. Bunsenges. Phys. Chem.*, 1954, **58**, 25-39.
3. W. F. Claussen, *J. Chem. Phys.*, 1951, **19**, 259-260.
4. A. Müller and M. Henry, *Cr. Chim.*, 2003, **6**, 1201-1208.
5. J. L. Kuo and M. L. Klein, *J. Chem. Phys.*, 2005, **122**.
6. S. S. Lin, *Rev. Sci. Instrum.*, 1973, **44**, 516-517.
7. J. Q. Searcy and J. B. Fenn, *J. Chem. Phys.*, 1974, **61**, 5282-5288.
8. O. Echt, D. Kreisle, M. Knapp and E. Recknagel, *Chem. Phys. Lett.*, 1984, **108**, 401-407.
9. U. Nagashima, H. Shinohara, N. Nishi and H. Tanaka, *J. Chem. Phys.*, 1986, **84**, 209-214.
10. R. W. Bolander, J. L. Kassner and J. T. Zung, *J. Chem. Phys.*, 1969, **50**, 4402-4407.
11. J. L. Kassner and D. E. Hagen, *J. Chem. Phys.*, 1976, **64**, 1860-1861.
12. M. P. Hodges and D. J. Wales, *Chem. Phys. Lett.*, 2000, **324**, 279-288.
13. C. C. Wu, C. K. Lin, H. C. Chang, J. C. Jiang, J. L. Kuo and M. L. Klein, *J. Chem. Phys.*, 2005, **122**.
14. A. Khan, *Chem. Phys. Lett.*, 2000, **319**, 440-450.
15. T. Kus, V. F. Lotrich, A. Perera and R. J. Bartlett, *J. Chem. Phys.*, 2009, **131**, 104313.
16. S. S. Xantheas, *Can. J. Chem. Eng.*, 2012, **90**, 843-851.
17. K. Hansen, P. U. Andersson and E. Uggerud, *J. Chem. Phys.*, 2009, **131**.
18. A. S. Zatula, M. J. Ryding, P. U. Andersson and E. Uggerud, *Int. J. Mass Spectrom.*, 2012, **330**, 191-199.
19. K. Honma and P. B. Armentrout, *J. Chem. Phys.*, 2004, **121**, 8307-8320.
20. P. U. Andersson, M. J. Ryding, O. Sekiguchi and E. Uggerud, *Phys. Chem. Chem. Phys.*, 2008, **10**, 6127-6134.
21. M. Miyazaki, A. Fujii, T. Ebata and N. Mikami, *Science*, 2004, **304**, 1134-1137.
22. J. W. Shin, N. I. Hammer, E. G. Diken, M. A. Johnson, R. S. Walters, T. D. Jaeger, M. A. Duncan, R. A. Christie and K. D. Jordan, *Science*, 2004, **304**, 1137-1140.
23. J. A. Fournier, C. J. Johnson, C. T. Wolke, G. H. Weddle, A. B. Wolk and M. A. Johnson, *Science*, 2014, **344**, 1009-1012.
24. S. Wei, Z. Shi and J. A. W. Castleman, *J. Chem. Phys.*, 1991, **94**, 3268-3270.
25. Z. Shi, S. Wei, J. V. Ford and A. W. Castleman Jr, *Chem. Phys. Lett.*, 1992, **200**, 142-146.
26. K. Suhara, A. Fujii, K. Mizuse, N. Mikami and J. L. Kuo, *J. Chem. Phys.*, 2007, **126**.
27. Jmol: an open-source Java viewer for chemical structures in 3D. http://www.jmol.org/
28. A. S. Zatula, P. U. Andersson, M. J. Ryding and E. Uggerud, *Phys. Chem. Chem. Phys.*, 2011, **13**, 13287-13294.
29. M. J. Ryding, A. S. Zatula, P. U. Andersson and E. Uggerud, *Phys. Chem. Chem. Phys.*, 2011, **13**, 1356-1367.
30. M. J. Ryding, K. Ruusuvuori, P. U. Andersson, A. S. Zatula, M. J. McGrath, T. Kurtén, I. K. Ortega, H. Vehkamäki and E. Uggerud, *J. Phys. Chem. A*, 2012, **116**, 4902-4908.

31. M. J. Ryding, A. M. Jonsson, A. S. Zatula, P. U. Andersson and E. Uggerud, *Atmos. Chem. Phys.*, 2012, **12**, 2809-2822.
32. C. E. Klots, *Z Phys. D Atom. Mol. Cl.*, 1987, **5**, 83-89.
33. K. Aidas, C. Angeli, K. L. Bak, V. Bakken, R. Bast, L. Boman, O. Christiansen, R. Cimiraglia, S. Coriani, P. Dahle, E. K. Dalskov, U. Ekström, T. Enevoldsen, J. J. Eriksen, P. Ettenhuber, B. Fernandez, L. Ferrighi, H. Fliegl, L. Frediani, K. Hald, A. Halkier, C. Hättig, H. Heiberg, T. Helgaker, A. C. Hennum, H. Hettema, E. Hjertenaes, S. Høst, I. M. Hoyvik, M. F. Iozzi, B. Jansik, H. J. A. Jensen, D. Jonsson, P. Jørgensen, J. Kauczor, S. Kirpekar, T. Kjærgaard, W. Klopper, S. Knecht, R. Kobayashi, H. Koch, J. Kongsted, A. Krapp, K. Kristensen, A. Ligabue, O. B. Lutnæs, J. I. Melo, K. V. Mikkelsen, R. H. Myhre, C. Neiss, C. B. Nielsen, P. Norman, J. Olsen, J. M. H. Olsen, A. Osted, M. J. Packer, F. Pawlowski, T. B. Pedersen, P. F. Provasi, S. Reine, Z. Rinkevicius, T. A. Ruden, K. Ruud, V. V. Rybkin, P. Salek, C. C. M. Samson, A. S. de Merás, T. Saue, S. P. A. Sauer, B. Schimmelpfennig, K. Sneskov, A. H. Steindal, K. O. Sylvester-Hvid, P. R. Taylor, A. M. Teale, E. I. Tellgren, D. P. Tew, A. J. Thorvaldsen, L. Thøgersen, O. Vahtras, M. A. Watson, D. J. D. Wilson, M. Ziolkowski and H. Ågren, *Wires. Comput. Mol. Sci.*, 2014, **4**, 269-284.
34. P. J. Stephens, F. J. Devlin, C. F. Chabalowski and M. J. Frisch, *J. Phys. Chem.*, 1994, **98**, 11623-11627.
35. S. Grimme, S. Ehrlich and L. Goerigk, *J. Comput. Chem.*, 2011, **32**, 1456-1465.
36. M. M. Francl, W. J. Pietro, W. J. Hehre, J. S. Binkley, M. S. Gordon, D. J. Defrees and J. A. Pople, *J. Chem. Phys.*, 1982, **77**, 3654-3665.
37. T. Clark, J. Chandrasekhar, G. W. Spitznagel and P. V. Schleyer, *J. Comput. Chem.*, 1983, **4**, 294-301.
38. V. Bakken and T. Helgaker, *J. Chem. Phys.*, 2002, **117**, 9160-9174.
39. R. Lindh, A. Bernhardsson, G. Karlstrom and P. A. Malmqvist, *Chem. Phys. Lett.*, 1995, **241**, 423-428.
40. F. Weigend and R. Ahlrichs, *Phys. Chem. Chem. Phys.*, 2005, **7**, 3297-3305.
41. S. Reine, A. Krapp, M. F. Iozzi, V. Bakken, T. Helgaker, F. Pawlowski and P. Salek, *J. Chem. Phys.*, 2010, **133**, 044102.
42. P. Merlot, R. Izsák, A. Borgoo, T. Kjærgaard, T. Helgaker and S. Reine, *J. Chem. Phys.*, 2014, **141**, 094104.